

Reconfigurable Modular Chain: A Reversible Material for Folding Three-Dimensional Lattice Structures

Zhe Xu

Mem. ASME
Department of Mechanical Engineering,
Yale University,
New Haven, CT 06511
e-mail: zhe.xu@yale.edu

Connor McCann

Department of Mechanical Engineering,
Yale University,
New Haven, CT 06511
e-mail: connor.mccann@yale.edu

Aaron M. Dollar

Mem. ASME
Department of Mechanical Engineering,
Yale University,
New Haven, CT 06511
e-mail: aaron.dollar@yale.edu

A wide range of engineering applications, ranging from civil to space structures, could benefit from the ability to construct material-efficient lattices that are easily reconfigurable. The challenge preventing modular robots from being applied at large scales is mainly the high level of complexity involved in duplicating a large number of highly integrated module units. We believe that reconfigurability can be more effectively achieved at larger scales by separating the structural design from the rest of the functional components. To this end, we propose a modular chain-like structure of links and connector nodes that can be used to fold a wide range of two-dimensional (2D) or three-dimensional (3D) structural lattices that can be easily disassembled and reconfigured when desired. The node geometry consists of a diamond-like shape that is one-twelfth of a rhombic dodecahedron, with magnets embedded on the faces to allow a forceful and self-aligning connection with neighboring links. After describing the concept and design, we demonstrate a prototype consisting of 350 links and experimentally show that objects with different shapes can be successfully approximated by our proposed chain design. [DOI: 10.1115/1.4035863]

1 Introduction

Self-reconfigurable modular robots contain a number of identical unit modules and are generally intended to change shapes and functions through reconfiguring their modules for different applications. However, this desirable reconfigurability comes with a high cost since each individual module requires independent actuation, communication, power, and even sensing. We believe that the benefits of reconfigurability do not have to be bonded to complicated modular robot designs that generally require a high degree of integration and miniaturization of both mechanical and electronic components. Instead, we argue that some of the intended benefits can be achieved by developing low-cost, lightweight, and reconfigurable modular materials that can be repeatedly used to construct the skeleton of different structures without

requiring individual sensing/actuation, but can instead be robotically assembled/disassembled.

The general approach of our proposed method is based on a concept in which a continuous prefabricated chain of links is deposited and connected to itself at joint nodes, producing structural lattices in nearly arbitrary configurations that can be disassembled and reconfigured when desired. Our design concept can be seen as a sort of 3D printer for sparse lattices, in which a robotic manipulator arm/small construction robot lays down/carries the links of a passive (nonrobotic) continuous chain to create programmed truss lattices using a hierarchy of submodules all formed from a single chain of links and joints. The concept will be similar to modern 3D printers that lay down a heated and extruded thread of acrylonitrile butadiene styrene (ABS) thermoplastic (i.e., fused deposition modeling) onto a substrate to create arbitrary 3D structures. Instead, we will lay down a chain of rigid links and joints (with appropriately designed connectors) to create lattice structures. To ensure rigidity, subunits consisting of links folded into planar triangles will be built upon and used to form three-dimensional rigid substructures, which will be expanded to produce “large” (i.e., many-unit) target three-dimensional structures, all using a single, compact, general-purpose platform.

The concept provides a means of custom fabrication of structural trusses and lattices based on a simple and generic base material. By starting with a densely packed spool of linkage chain, structures can be efficiently “deployed” in customizable configurations and geometries to meet immediate fabrication needs, and then reused/reconfigured for successive applications (see Fig. 1). The approach can be implemented in any number of size scales and materials, thereby cutting across many application domains, from millimeter-scale segment lengths for small part construction, to meter-scale segments for civil structures.

In the following sections, we first review related work in Sec. 2, and then detail the important aspects of our design in Secs. 3 and 4. After this, two different prototyping processes are described in Sec. 4. We finish by estimating the mechanical properties of the assembled lattice structure and validating the efficacy of our proof-of-concept design by demonstrating the folding process of five basic geometries in Sec. 5.

2 Related Work

In order to position our proposed design concept, in this section we briefly review the previous works that are most relevant to our project. The existing limitations of these works are not meant to be critical, but rather served as the driving forces during the formation of our design concept.

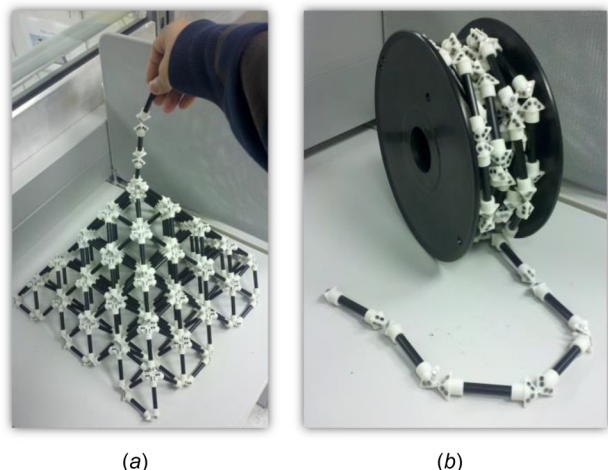


Fig. 1 Pictures of our proof-of-concept design: (a) 293 links are used in the folding of the pyramid shape and (b) a spool of the modular chain

Manuscript received October 7, 2016; final manuscript received January 13, 2017; published online March 9, 2017. Assoc. Editor: Hai-Jun Su.

2.1 Reconfigurable/Modular Robots. The primary motivation for our current work comes from modular robots, where repeating robotic submodules join together to form more complicated structures. A variety of modular robots has been successfully designed and prototyped in the past two decades. As thoroughly summarized in a recent review [1], although each of them possesses distinctive shapes and features, none of them were produced in large quantities, preventing researchers from fully exploring the possible applications of modular robots at a large scale.

Even if a number of modular robots can transform into a large robot/structure, a significant portion of these modular units will be required to serve as the internal structure maintaining the integrity of the entire shape. For those modules that are only used as support materials inside a larger robot/structure, it is a waste to equip them with the same number of sensors and actuators compared to the ones serving more functional purposes. In fact, the mechanical strength of those modular robots may have already been compromised when complicated electronics and actuators were densely packed inside them. This may prevent them from forming any large shape in the first place.

2.2 Swarm Robots. Similar to modular robots, robotic swarms utilize large numbers of simple, independent robotic members to work in tandem to achieve a goal. Recently, over a thousand swarm robots have been deployed to demonstrate impressive assembly behaviors on a 2D surface [2]. The large number of these robots makes the entire system a good resource to investigate how biological assembly occurs in nature. For the purpose of building 3D structures, however, these swarm robots cannot use themselves as the building blocks, but have to carry and manipulate separate construction materials from somewhere else. Manipulation and assembly tasks have been previously demonstrated with swarm robots; however, even the simple case of assembling two mating parts in 2D took over an hour for a swarm to complete [3]. While highly distributed tasks among many collaborative agents might be an optimum solution to collect materials and build different types of habitats in nature, such an approach may not be suitable for robotic construction of large structures using prefabricated modular building blocks.

2.3 Origami-Inspired Folding. One possible solution to the shortcomings of modular and swarm robots is to integrate the reconfigurability into a single robotic module, such as is done with origami-inspired panel folding, where a structure is fabricated with preset creases so as to form a 3D shape when activated. Deployable origami structures can realize the reversible transformation between 2D and 3D shapes [4], though sandwiching techniques are often required in order to make the folded 3D structure strong enough to withstand external loads [5]. In addition, once the mountain/valley creases are determined, the bistate feature of the origami folding only allows the 2D panel to form a designated 3D structure, unlike modular robots that can form numerous configurations.

Compared to origami folding, our proposed method allows reversible transformations between 1D chain, 2D plane, and 3D lattice structures, which further improves the compactness and flexibility of the folding technique.

2.4 Additive Manufacturing. Another way to achieve arbitrary spatial geometries is additive manufacturing, such as 3D-printing, that allows the fabrication of complex shapes from a simple base material (typically ABS). Although different sparse in-fill patterns have been designed in order to save materials and prototyping time [6], 3D printers generally print parts that are greater than 50% density and require hours of operation for prototyping centimeter scale parts.

Although the convenience of making personalized parts can be achieved, the prototyping process of additive manufacturing is

irreversible, making it nearly impossible to recycle the materials or change the design on the fly.

2.5 Programmable Matter and Cellular Materials. Research into programmable matter seeks to combine the best properties from each of these previously explored concepts (namely reconfigurability, speed, and high strength/weight ratios). The concept of the programmable matter is that the same amount of the material can be used to form different shapes without being consumed by the formation of any permanent fixed structure [7]. However, most of these design concepts are still at the simulation stage and can only be demonstrated with magnetic fluid [8,9].

On the other hand, cellular materials—the closest counterparts of programmable matter that currently exist—have demonstrated appealing mechanical properties by assembling a number of strong but lightweight carbon fiber struts into a lattice structure [10]. The resulting structure not only exhibits very large Young's modulus at low density, but also requires high assembly/disassembly precision.

3 Converting 2D/3D Shapes Into Rigid Lattice Structures

When designing the basic shape of modular robots, regular polyhedra such as the cube are often chosen [11], since the equal sides reduce design complexities and allow individual modules to couple with neighboring units with less uncertainty. Similarly, we use a fixed link-length for the basic module of our proposed reconfigurable modular chain. The lattice structure constructed by our proposed modular chain is called an octet-truss [12] and can be used to approximate the shape of 3D objects. The selection of this unique lattice structure is closely related to the fundamental problem of finding tiling patterns for 2D/3D tessellation. This section details this important design process.

In theory, the task of using a number of identical modules to form or approximate any target shape can be treated as a 2D/3D tessellation problem, since the shape of each modular unit can be seen as the periodic tiling unit used for filling the target shape in 2D/3D situations. In the case of tiling planar shapes in 2D Euclidean space, three regular polygons, namely regular triangles, squares, and hexagons, have been identified as the basic building blocks. In practice, these shapes have been typically realized as triangular prisms and cubes, and have been widely adopted as the basic configurations of modular robots to generate 2D shapes [11]. In contrast, tessellation in 3D Euclidean space is still an ongoing field of research and has not yet been completely solved [13]. To date, cubes are the only regular polyhedron known to be able to tessellate in 3D Euclidean space.

Since our goal is to use the reconfigurable chain to form 2D/3D lattice structures, we need to further decompose the 2D/3D shapes that are made up of regular polygons/polyhedra into lattice structures that are comprised of struts of equal length. This solid-to-lattice conversion process simply involves removing all the faces, keeping the edges of each building block. In the 2D case, regular triangles can be easily used to convert planar shapes into lattice structures with good mechanical rigidity (see Fig. 2(a)) [14]. However, in the 3D case, the resulting lattice structure extracted from a solid cube is not rigid according to the Maxwell criterion (see Fig. 2(b)) [15]

$$\text{No. of edges} = 3 * \text{No. of nodes} - 6 \quad (1)$$

In order to resolve this problem, we can first find the dual of the solid cube—which is an octahedron with six vertices coinciding with the face centers of the cube (see Fig. 3(a)) and then fill the gaps between octahedra with tetrahedra that have the same edge lengths as shown in Fig. 3(b). This unique combination of the alternating octahedra and tetrahedra (with a ratio of 1:2) is known as the tetrahedral–octahedral honeycomb, which can also be used

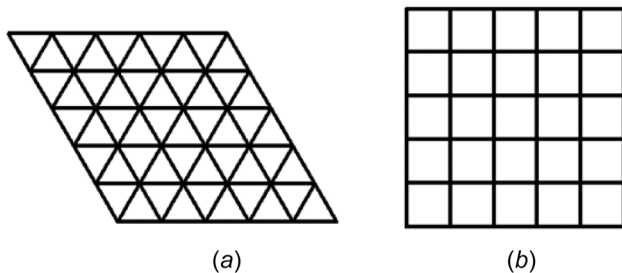


Fig. 2 Top views of the tiling patterns in 2D and 3D situations: (a) using regular triangle-lattices to construct 2D shapes and (b) using cube-lattices to construct 3D shapes

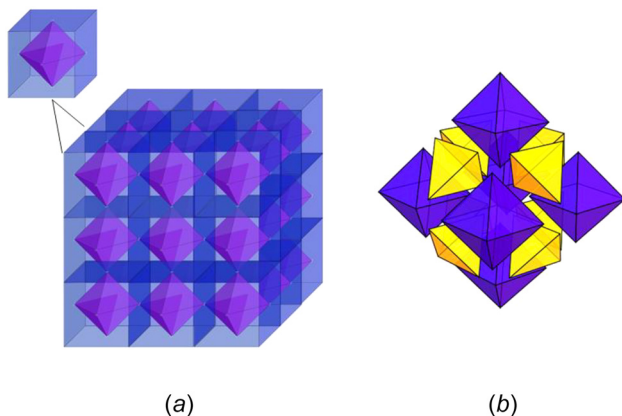


Fig. 3 Tessellation of 3D space with regular octahedra and tetrahedra

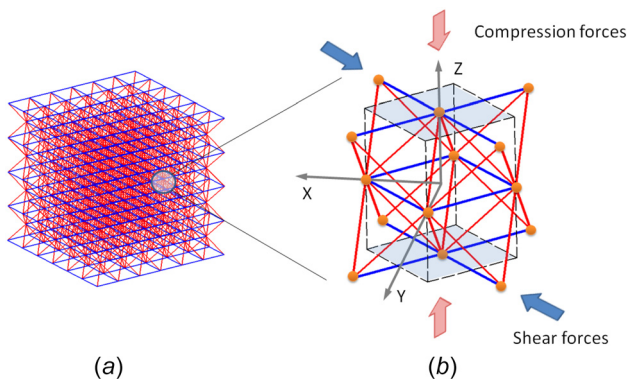


Fig. 4 Schematic drawing showing the lattice structure (left) and its unit cell after the solid-to-lattice conversion of a cube (right). Note: the arrows illustrate the loading orientations of the compressive and shear forces that act on the shaded top and bottom planes.

to tessellate in 3D Euclidean space. After going through the same solid-to-lattice conversion process, the resulting lattice structure consists of a series of tightly packed unit cells as shown in Fig. 4 (left). It is worth mentioning here that the periodic unit cell replaces the exact space previously occupied by the original solid cube as illustrated in Fig. 4 (right).

It is interesting to note that although neither octahedrons nor tetrahedrons alone are space filling shapes, the structure of the combined unit cell is not only a 3D tiling pattern, but also satisfies the Maxwell criterion. In terms of its mechanical property, the unit cell has been proven to be stretch-dominated and therefore is more weight-efficient for structural applications than bend-dominated structures [15].

4 Design of the Reconfigurable Chain

In this section, we systematically unfold the important design considerations of our reconfigurable modular material from three different aspects, namely the basic chain structure, the shape of the node, and the coupling methods between neighboring links.

4.1 Three-Dimensional Structure Formed by an Eulerian Path. In our design, we propose to fold the target structure with a lightweight, but inherently strong truss structure. Our previous work has proved that any arbitrary 2D shape can be approximated by folding strings along a semi-Eulerian path [14]. A previous work on sequential folding or modular assembly [16] was mainly inspired by deoxyribonucleic acid origami at the nanometer scale [17]. In order to design materials that possess good weight/load ratios and reconfigurability, recent efforts have been mainly focused on origami folding of 2D sheets [18,19] or robotic assembly of discrete materials [20,21].

We intentionally introduce mechanical constraints into the system by chaining up a series of identical links. The advantage is twofold: first, each individual link can easily locate its global position based on its piecewise information relative to its neighboring links saving the need of local sensing. Second, from a practical point of view, during the assembly and disassembly process, a piece of continuous 1D chain provides a friendly infrastructure to organize deployment/storage of the used/unused units (links).

4.2 Geometry of the Node. As shown in Fig. 1, regardless of the final size of the target truss structures, they all share the same types of joint connections where the chain of links meets itself at joint nodes. To meet this requirement, each link of the chain should contain two identical nodes at the ends of one common rod (see Fig. 5 top right). Depending on the planning algorithm, different arrangements of the nodes can form different types of joints inside a large three-dimensional lattice structure (as shown in Fig. 5 left). Theoretically, the busiest joint may need to connect as many as 12 links through 12 identical nodes. Based on their different functions in the lattice structure, the rods at the joint can be further categorized into contour and fill layers (see Fig. 5 middle).

If we remove all the rods from the busiest joint and only leave the nodes with all the connecting sites exposed, the resulting joint can be geometrically represented as a 12-sided rhombic dodecahedron (see Fig. 5 right). Similarly, any other joint configuration can be seen as a partially formed set of 12 (the busiest joint) with some number of nodes missing. In this way, in order to design the basic shape of each individual node, we need to find a solution to cut the 12-sided rhombic dodecahedron into 12 identical shapes so that each of them can be used as the generic shape for the connector node.

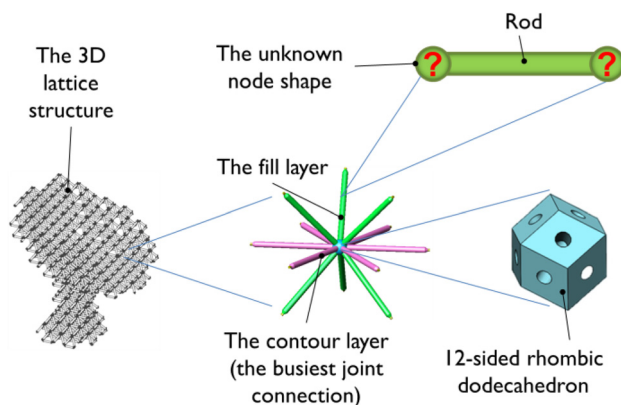


Fig. 5 Schematic drawing showing the different components at the busiest connection joint inside a large three-dimensional lattice structure (an antenna frame)

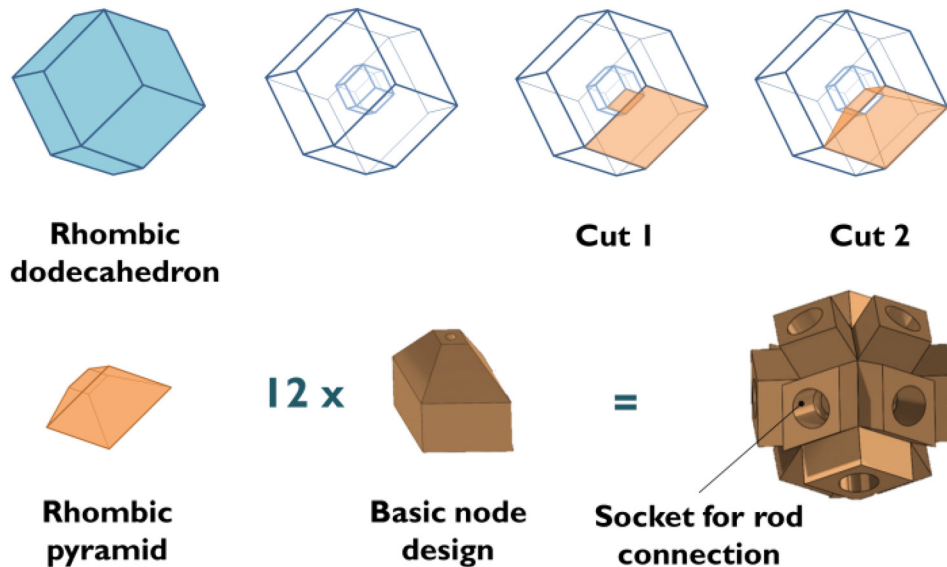


Fig. 6 The formation of the basic node geometry. Top row: a smaller rhombic dodecahedron is first fit into the center of the busiest connection joint. Bottom row: after a series of cutting processes, the rhombic pyramid shape is selected to form basic geometry of node design.

The cutting process can be divided into two steps. As shown in the top row of Fig. 6, the edge length of the original rhombic dodecahedron is a . First, a small rhombic dodecahedron (with edge length equals a/n , $n > 1$) is concentrically placed inside the original one. And then, the four vertices from one face of the small rhombic dodecahedron are connected with the corresponding vertices from the outside rhombic dodecahedron. The shape bounded by the two faces and four edges is a rhombic pyramid. It has four symmetrically identical faces and is hereinafter used as the basic shape for our node design.

After adding a simple base with a socket for the rod connection, 12 of these rhombic pyramid nodes can seamlessly form the busiest connection joint without any assembly issues (see Fig. 6 bottom row). Although we found other basic shapes that can also be used to construct the node and form the same joint, the rhombic pyramid shape allows us to maximize the contact area between the neighboring nodes.

As the uniformly extruded rod is inherently stronger and stiffer than the connection joints inside a reconfigurable lattice structure, the contact area between the two nodes is critical to the stability of the entire structure. Since our proposed design is aiming to implement reconfigurability into the structures that are at either small or large scale, we are interested in knowing how the size of the node design can affect the contact area between nodes.

As shown in Fig. 7, the two opening angles at the base of the rhombic pyramid are

$$\alpha = \sin^{-1} \left(\frac{\sqrt{6}}{3} \right) \quad (2)$$

$$\beta = \sin^{-1} \left(\frac{\sqrt{3}}{3} \right) \quad (3)$$

with the height

$$h = \frac{\sqrt{6}a}{3} \quad (4)$$

we can calculate the edge lengths as follows:

$$b = \sqrt{(a * \sin \beta)^2 + h^2} = a \quad (5)$$

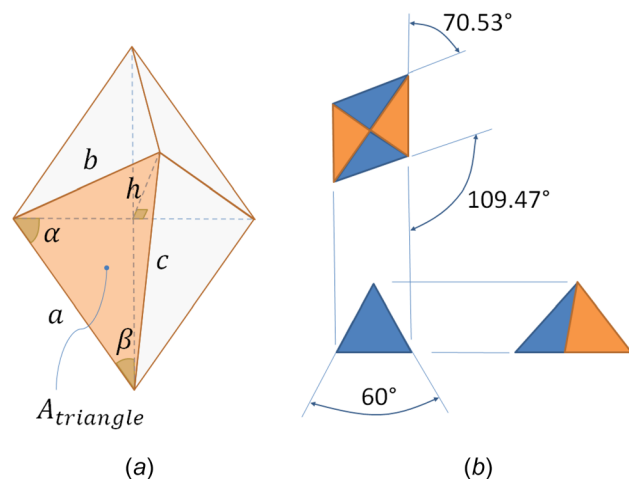


Fig. 7 The important dimensions of our node design: (a) the rhombic pyramid with four symmetrically identical faces and (b) schematic drawing of the node design showing the critical assembly angles

$$c = \sqrt{(a * \sin \alpha)^2 + h^2} = \frac{\sqrt{12}a}{3} \quad (6)$$

Based on Heron's formula, the area of the shaded triangle can be calculated based on the lengths of its sides by using the following equation:

$$A_{\text{triangle}} = \sqrt{s(s-a)(s-b)(s-c)} = \frac{\sqrt{2}a^2}{3} \quad (7)$$

where $s = (a + b + c)/2$ is defined as the semiperimeter of the shaded triangle.

Therefore, the area for coupling contact A and volume V of the rhombic pyramid are

$$A = 4 * A_{\text{triangle}} = \frac{4\sqrt{2}a^2}{3} \quad (8)$$

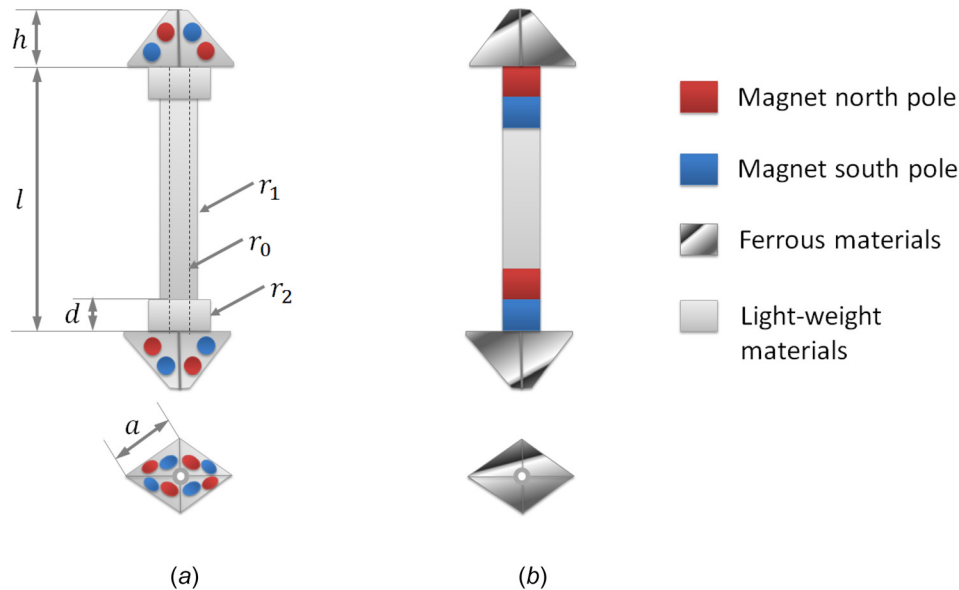


Fig. 8 Two different types of magnetic coupling used in our prototype: (a) type-I—embedding paired magnets directly at the contacting sites and (b) type-II—transmitting magnetic forces through the node made of ferrous materials. Note: the central hole is for anchoring connecting strings.

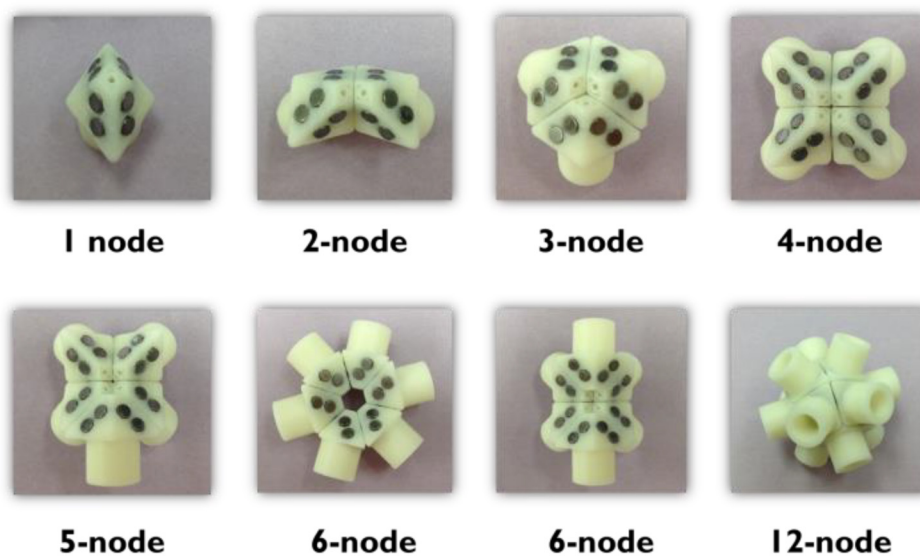


Fig. 9 Possible connection joints supported by type-I coupling method. Note: except for the start and the end, all the other connection joints have even number of nodes inside any folded lattice structure. Rods were removed for better visibility of the nodes.

$$V = \frac{4\sqrt{3}a^3}{27} \quad (9)$$

Besides distributing and guiding the contact forces, the plain contact surfaces themselves cannot directly provide any coupling forces between neighboring nodes. However, its size determines the type of the latching mechanism that can be implemented in order to provide the required coupling forces. Therefore, these two parameters (A and V) are important design factors.

4.3 Connection Between the Nodes. The coupling between adjacent nodes is the key to maintaining the rigidity of the reconfigurable lattice structure. Depending on the size of the resulting

link design, there are two major locations that can be potentially used to incorporate different coupling methods as shown in Fig. 8.

When the size of the target structure is larger than the centimeter scale, the type-I method is a good option since contact sites are abundant for implementing different types of surface features for latching mechanisms [1]. Currently we chose small neodymium magnets (3.2 mm in diameter, 1.6 mm in thickness, N52 grade) to validate our design concept due to their easy implementation, good strength (2.5 N magnet–magnet pulling forces), and self-alignment features.

As shown in Fig. 9, the four faces of the rhombic pyramid provide an ideal platform for the alternating male–female coupling pattern. Different types of connection joints can be easily formed upon contact.

As the size of the target structure gets smaller than the centimeter scale, the size of the node and rod will also need to be reduced

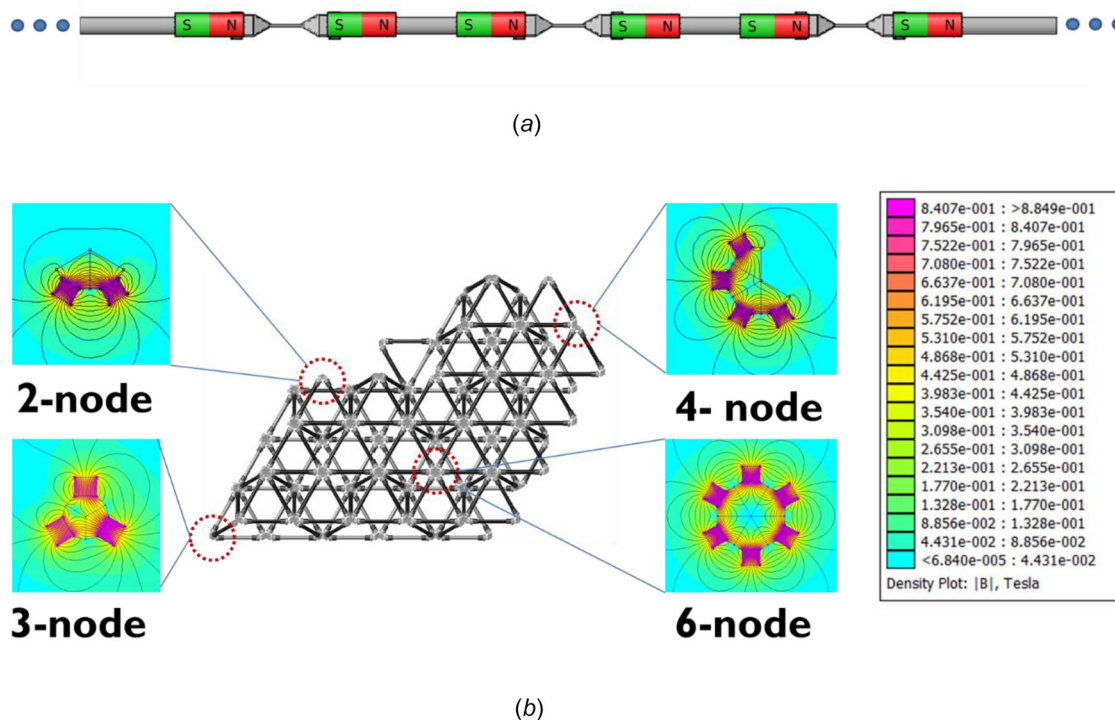


Fig. 10 Two-dimensional simulation of the magnetic fields by using type-II coupling method: (a) alternating the poles at the two ends of each rod and (b) 2D simulation of the magnetic fields at different connection joints in a 3D reconfigurable lattice structure

accordingly. Therefore, fewer contact surfaces will be available for implementing type-I coupling and the locations of the coupling sites need to be further pushed back toward the middle of the rod. In this case, adopting type-II coupling methods can be a good way to latch the two adjacent nodes. To this end, magnets with alternating poles can be directly attached to the ends of a rod leaving the contact sites between nodes plain, as long as the nodes are made of ferrous materials that possess good magnetic permeability. Simulation of the magnetic field confirmed that the resulting magnetic forces can aid the formation of different joints inside a folded 3D structure (see Fig. 10).

It is important to recall that our proposed folding path follows a semi-Eulerian path, and therefore except for the start and end, all the connection joints have even number of nodes to allow pairing between alternating poles.

Although we used permanent magnets for both of the two coupling methods, the same idea can be upgraded to incorporate a variety of controllable interlocking/latching mechanisms, e.g., electropermanent magnetic connectors [22], mechanical latching mechanisms [23,24], and even reversible soldering connectors [1].

5 Fabrication Process

As will be demonstrated in the Experimental section, our proposed modular material requires hundreds of links during the folding process. Based on the two different types of coupling methods, we also experimentally explored two rapid prototyping methods in order to maximize their performance in different application scenarios. We believe a good all-around design should also consider the manufacturing methods.

The type-I coupling method has the magnetic latching mechanism directly embedded at the contact sites. Therefore, it does not require special materials for the nodes. As shown in Fig. 11, an array of 110 nodes can be printed in 36 h by using Stratasys's μ Print. Each individual link weights 5.7 g and is composed of two 3D printed nodes and a 53 mm long ABS tube. As shown in Figs. 11(c) and 11(d), one chain can be folded into a variety of

objects—including 2D and 3D shapes—with only 14 links. It is important to point out that incremental rigidity of the assembled structure is achieved by sequentially folding triangles during the entire folding process [14].

As discussed in Sec. 4.3, type-II coupling requires ferrous materials with good magnetic permeability to allow the transmission of the magnetic fields between neighboring nodes. Instead of using computer numeric control (CNC) machined metal nodes, we found that a cold-casting method can enable us to cost-efficiently fabricate a large number of ferrous parts with good precision in a short period of time (see Figs. 12(a)–12(c)). Cold-casting is a well-established molding technique involving mixing epoxy resins with a small amount of metal powder and is mainly used by artists to fabricate metallic-looking statues at low cost. In our case, we used a high metal–resin volume ratio (99.9% iron powder/epoxy resin $> 7:1$) and therefore each cold-casted node weights around 1.2 g—only 18.2% of the CNC machined one—but can still effectively direct magnetic flux as well as the CNC machined one as shown in Fig. 12(d).

However, compared to the 3D printing method used by our type-I node design, the cold-casting method needs two separate molding processes for the silicone mold and final parts, respectively. At our current design stage, the latter requires more manual work and prototyping time. Therefore, in order to efficiently demonstrate our proof-of-concept design, we chose type-I nodes for the rest of the experiments.

6 Experimental Evaluation and Predictions of Mechanical Properties

6.1 Prototype of Modular Chains. In order to demonstrate the reconfigurability of our proposed design, we prototyped 350 links (700 nodes) based on the type-I coupling method due to its relatively efficient prototyping process. The resulting modular chain can be compactly organized and stored by using a spool

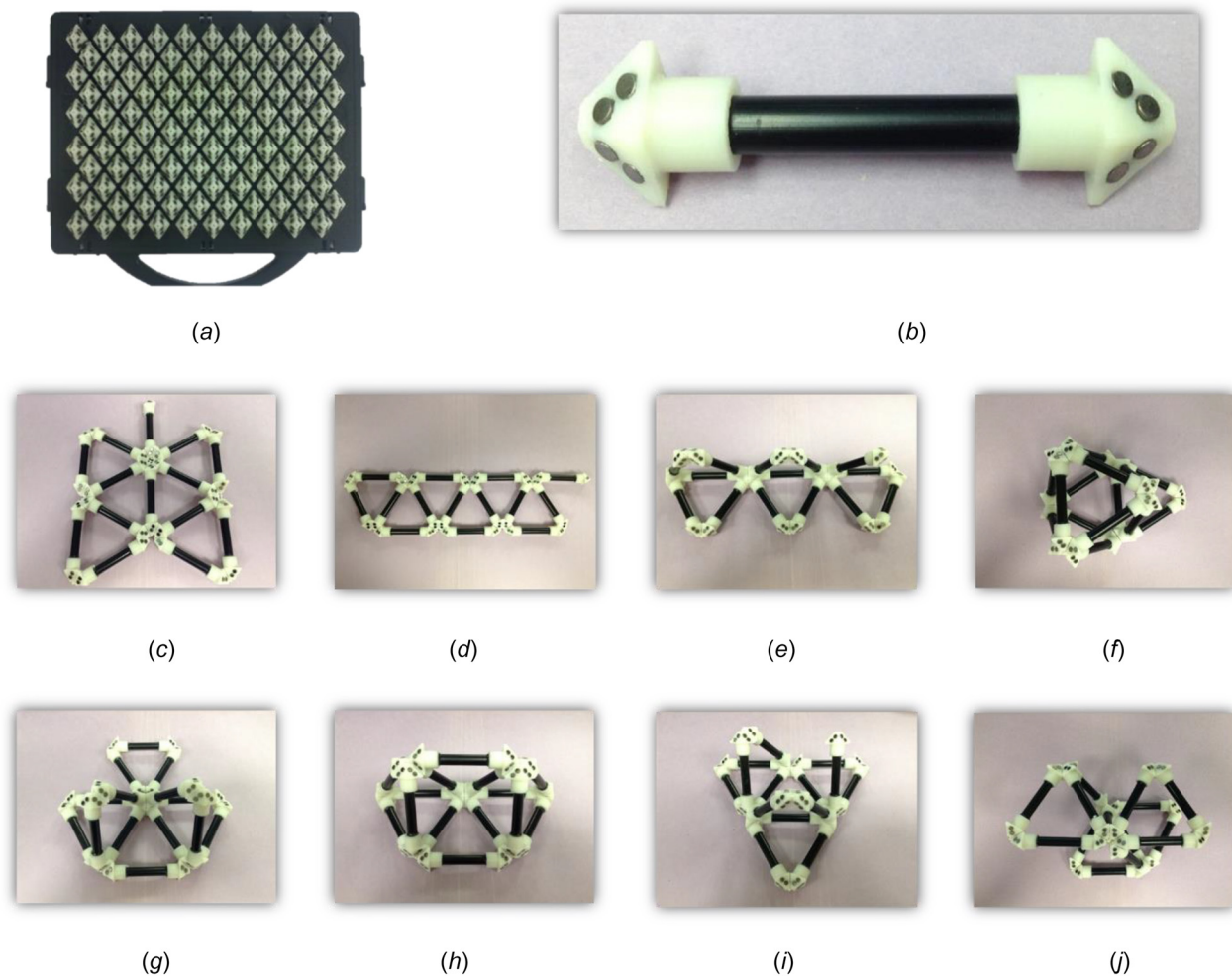


Fig. 11 The prototyping process of nodes via 3D printing: (a) a tray of 110 3D-printed nodes, (b) example of a separate link, and (c)–(j) variations of 2D and 3D structures folded by a 14-link chain

(see Fig. 1(b)) and folded into a variety of shapes by following different folding paths as demonstrated in Figs. 13 and 14.

In contrast to hours of fabrication time required by 3D-printing processes, once the folding path of a target structure is planned, all of our demonstrated structures can be quickly folded in a few minutes. In addition, the disassembly process takes even less time since the chain structure can automatically guide the unfolding process by moving from one unlatched link to the other sequentially.

As shown in Fig. 15, our design concept can also be scaled up to form much larger structures. The reconfigurability of the chain structure allows the same number of links (1554 of 0.3 m strut) to be constructed into either two solar panels or one antenna frame. Since the links are all connected by compliant strings in a piecewise manner, the extra/excessive links can be easily attached/removed. In this case, the shell of a space habitat can be built by extending the chain to 7560 links.

With an active cell mechanism [25], the chain can also morph into a shorter one, so that smaller structures can also be formed without the need to changing the chain. If we reduce the length of each link to half its original length and remove 3534 links, the same chain can be used to form the chassis of a planetary rover.

6.2 Relative Density and Predictions of Mechanical Properties. The relative density of the octet-truss, which is denoted by $\bar{\rho}$, is the ratio of the density of the lattice structure (the

unit cell) to the density of the solid materials used to build the lattice. It can be calculated by using the following equation:

$$\bar{\rho} = \frac{m/v_{\text{cell}}}{m/v_{\text{strut}}} = \frac{v_{\text{strut}}}{v_{\text{cell}}} \quad (10)$$

where m is the mass of the lattice structure, v_{cell} is the volume of the bounding box (marked by dashed lines in Fig. 4) of the unit cell, and v_{strut} is the sum of the volumes of struts enclosed in the bounding box. The values of v_{cell} and v_{strut} can be calculated with the following equations:

$$v_{\text{cell}} = \sqrt{2}(l + 2h)^3 \quad (11)$$

$$v_{\text{strut}} = 12v_{\text{link}} = 12 \cdot (2v_{\text{node}} + v_{\text{rod}}) \quad (12)$$

$$v_{\text{rod}} = \pi(r_1 - r_0)^2 l \quad (13)$$

$$v_{\text{node}} = \frac{4\sqrt{3}a^3}{27} + \pi(r_2 - r_1)^2 d \quad (14)$$

where r_0 , r_1 , and r_2 are the inner radius of the rod, outer radius of the rod, and outer radius of coupling flange, respectively. Additionally, l is the length of the rod and d is the height of the coupling flange as shown in Fig. 8(a). The values of these design parameters are listed in Table 1. Substituting these values and Eqs. (11)–(14) into Eq. (10), the relative density becomes

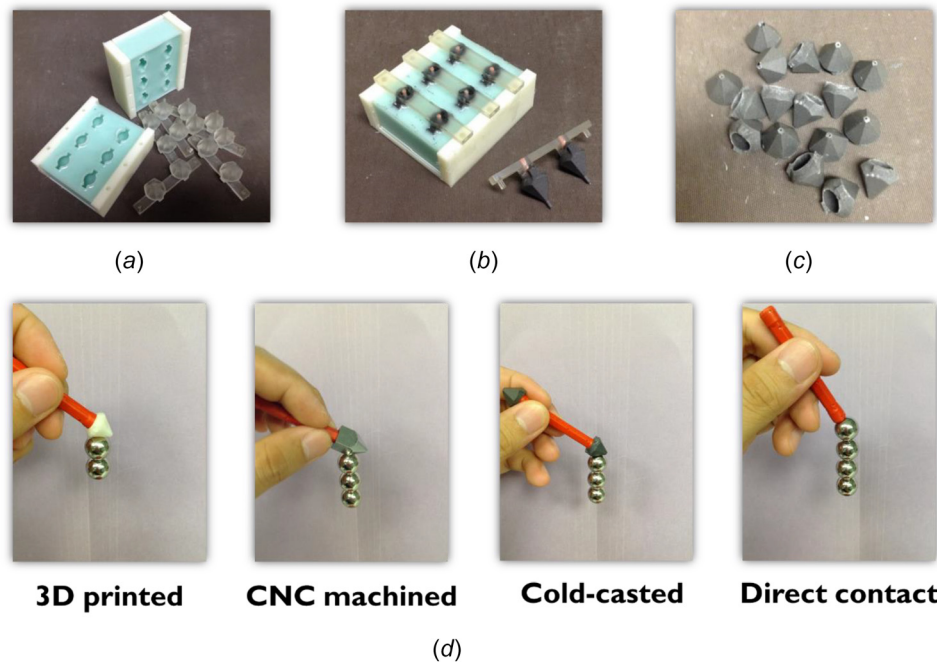


Fig. 12 Prototyping process of nodes by using cold-casting method: (a) 3D-printed positives and the silicone rubber mold, (b) and (c) cold-casted parts made from the mixture of fine iron powder and resins, and (d) comparison of magnetic forces with nodes made of different materials. Note: each steel ball weights 8.4 g. The rod is the off-the-shelf Geomag part.

$$\bar{\rho} = \frac{12 \cdot (2v_{\text{node}} + v_{\text{rod}})}{\sqrt{2}(l + 2h)^3}$$

$$= \frac{6\sqrt{2} \left(\frac{8\sqrt{3}a^3}{27} + 2\pi(r_2 - r_1)^2 d + \pi(r_1 - r_0)^2 l \right)}{(l + 2h)^3} \approx 1.66\%$$
(15)

Without considering the shape and volume of the node ($a = 0$, $d = 0$, $h = 0$, $r_2 = 0$), and only using solid struts ($r_0 = 0$), the relative density takes the form $\bar{\rho} = 6\sqrt{2}\pi(r_1/l)^2$, which has been used for idealized lattice structures [26]. This equation slightly overestimates the relative density, however, because of the double-counting of the volume overlap at the nodes.

Relative density is an important material parameter in the elastic compliance matrix. As shown in Fig. 3, the cubic symmetry property of the octet-truss lattice suggests the following linear elastic strain (ϵ_{ij}) and stress (σ_{ij}) tensor relationship [26] for pin-jointed struts (indices i, j are defined based on the coordinate system described in Fig. 4)

$$\begin{pmatrix} \epsilon_{xx} \\ \epsilon_{yy} \\ \epsilon_{zz} \\ \epsilon_{yz} \\ \epsilon_{xz} \\ \epsilon_{xy} \end{pmatrix} = \frac{1}{\bar{\rho}E_s} \begin{pmatrix} 9 & -3 & -3 & 0 & 0 & 0 \\ -3 & 9 & -3 & 0 & 0 & 0 \\ -3 & -3 & 9 & 0 & 0 & 0 \\ 0 & 0 & 0 & 12 & 0 & 0 \\ 0 & 0 & 0 & 0 & 12 & 0 \\ 0 & 0 & 0 & 0 & 0 & 12 \end{pmatrix} \begin{pmatrix} \sigma_{xx} \\ \sigma_{yy} \\ \sigma_{zz} \\ \sigma_{yz} \\ \sigma_{xz} \\ \sigma_{xy} \end{pmatrix}$$
(16)

where E_s is the Young's modulus of the strut material (2.25 GPa for ABS materials).

Based on our current folding method as briefly described in Fig. 13, our 3D lattice structures (see Fig. 14) are designed to support external loads mainly from their top; therefore, the

mechanical properties of our lattice structures along the z direction is of the greatest interest (see Fig. 4). From Eq. (16), the following two stiffness predictions can be derived [27]:

For the compressive modulus

$$E_{zz} = \frac{1}{9}\bar{\rho}E_s \approx 4.15 \times 10^{-3} \text{ GPa}$$
(17)

For the shear modulus

$$G_{zx} = \frac{1}{12}\bar{\rho}E_s \approx 3.11 \times 10^{-3} \text{ GPa}$$
(18)

Based on the geometries of the node and unit cell as shown in Figs. 4 and 7, we can further derive the following relationships between the coupling forces and external forces for the unit cell under different loading conditions:

Under compression forces

$$F_{\text{compression}} = 4(F_{\text{strut}}^{\text{axial}} \sin 45 \text{ deg} + F_{\text{strut}}^{\text{radial}} \cos 45 \text{ deg})$$
(19)

Under shear forces

$$F_{\text{shear}} = 2\sqrt{2}(F_{\text{strut}}^{\text{axial}} \cos 45 \text{ deg} + F_{\text{strut}}^{\text{radial}} \sin 45 \text{ deg})$$
(20)

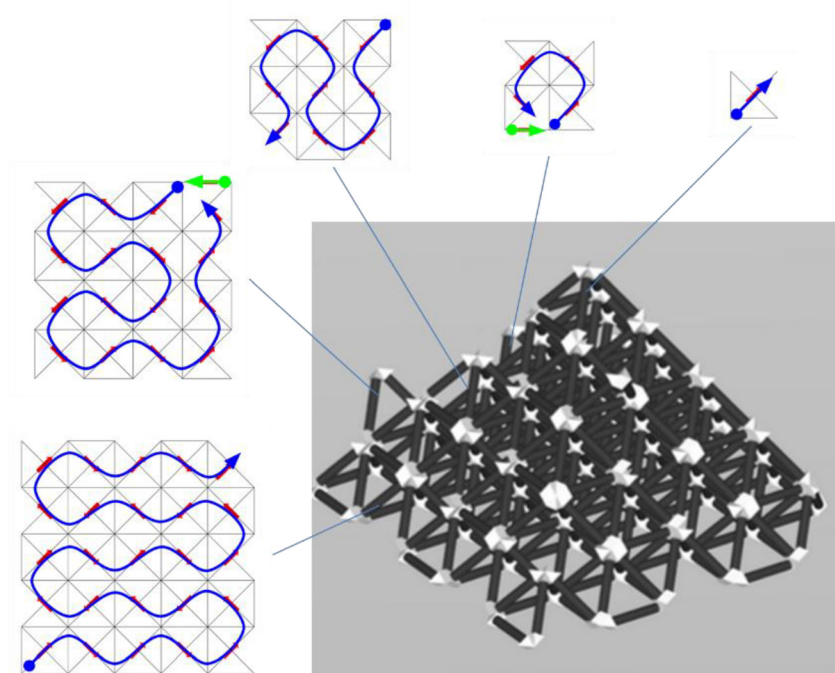
where $F_{\text{strut}}^{\text{axial}}$ and $F_{\text{strut}}^{\text{radial}}$ are the sum of coupling forces acting along the axial and radial directions of each link at the node joint, respectively. Once assembled, the string connection between neighboring links is similar to a pin-joint. Therefore, the contribution to the stiffness due to the bending of the struts is negligible [27]. And Eqs. (19) and (20) become the followings under the pin-joint assumption:

$$F_{\text{compression}} = 4F_{\text{strut}}^{\text{axial}} \sin 45 \text{ deg}$$
(21)

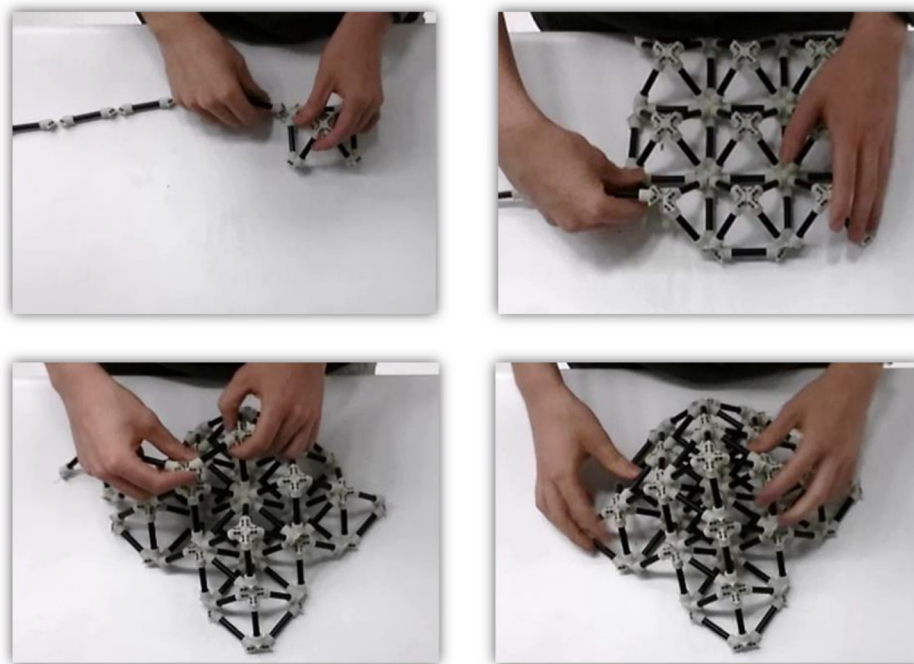
$$F_{\text{shear}} = 2\sqrt{2}F_{\text{strut}}^{\text{axial}} \cos 45 \text{ deg}$$
(22)

where

$$F_{\text{strut}}^{\text{axial}} = 4F_{\text{contact}} \sin 30 \text{ deg}$$
(23)



(a)



(b)

Fig. 13 Example of the folding process: (a) the separate folding paths for constructing different layers of a pyramid and (b) snapshots showing the demonstration of planned folding process

The contacting forces, F_{contact} , originate from the four faces of the rhombic pyramid node. In our current design, they equal to the magnetic forces from two the two pairs of neodymium magnets (5 N). Therefore, the current unit cell can approximately support either 28.3 N compression or 20 N shear forces. As we mentioned

previously, our current prototype is a proof-of-concept design; therefore, both the stiffness predictions (the compressive and shear moduli) and the predicted compression and shear forces will increase once we choose a stronger strut material and incorporate mechanical coupling methods into the node design.

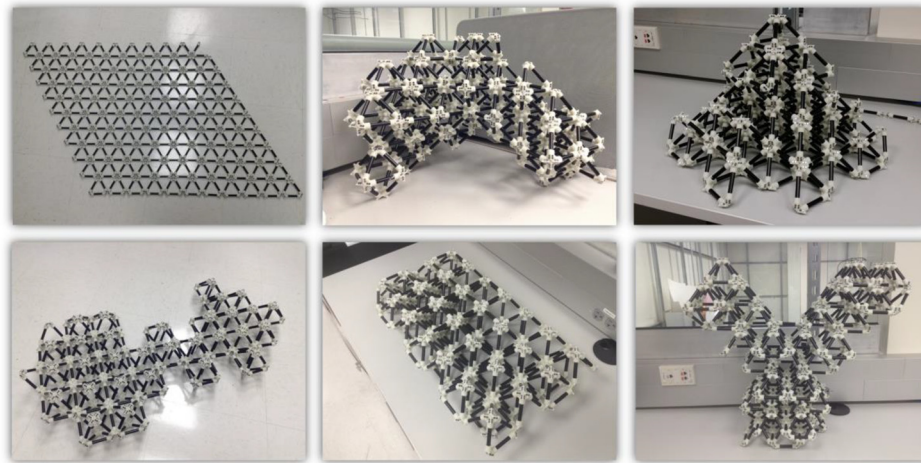


Fig. 14 Variations of folded shapes both in 2D and 3D (329-link)

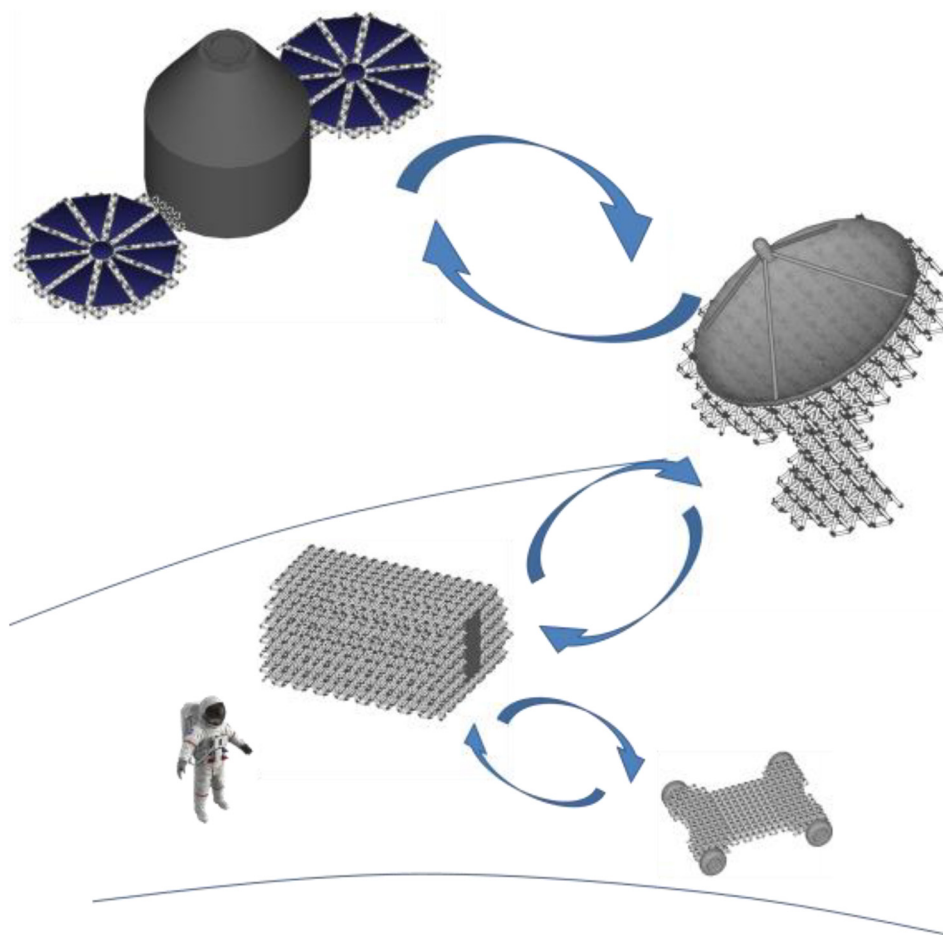


Fig. 15 Potential applications of our proposed chain design in space exploration. Note: the frames of the antenna and solar panel are all folded by the same chain with 1554 links.

Table 1 Node and rod dimensions for the modular chain (units: mm)

l	d	a	h	r_0	r_1	r_2
53.0	8.0	12.5	10.2	1.6	3.2	5.5

7 Conclusion and Future Work

We have designed and prototyped a new type of reconfigurable modular material that can be easily deployed/recycled to fold/unfold 3D lattice structures. Important design criteria were detailed about the shape of the nodes, the coupling between nodes, and the prototyping methods for two different types of magnetic

latching mechanisms. We experimentally demonstrated that our design can facilitate the formation of different connection joints needed for building 3D structures, and the reconfigurability of our design can be clearly observed in both small (14-link) and large (350-link) structures. Due to its light weight and low pre/postdeployed volume ratio, we believe that our proposed design will be beneficial to a number of applications, including space exploration, construction in remote environments, and others where material weight (and therefore reconfigurability) is at a premium.

In future work, we will further improve the strength of the coupling forces between connector nodes via mechanical latching mechanisms and experimentally test the mechanical properties of different design concepts, as well as designing algorithms for structures of varying lattice density and strength. We will also be developing a folding algorithm and working toward a robotic “printer” using the chain to autonomously lay down lattice components to construct structures of arbitrary desired shapes.

Acknowledgment

The authors would like to thank Devin Balkcom and Corey O’Hern for their input during the development of this concept. This work was supported in part by a NASA Early Career Faculty Award (Grant No. NNX14AO55G).

Nomenclature

a	= edge length of the rhombic dodecahedron
A	= area of the rhombic pyramid for coupling contact
A_{triangle}	= area of the shaded triangle
b	= edge length of the shaded triangle
c	= edge length of the shaded triangle
d	= height of the coupling flange
E_s	= Young’s modulus of the strut material
E_{zz}	= compressive modulus of the truss
$F_{\text{compression}}$	= compressive force supported by unit cell
F_{contact}	= total contact force at the nodes
F_{shear}	= shear force supported by the unit cell
$F_{\text{axial strut}}$	= sum of the coupling forces in the axial direction
$F_{\text{radial strut}}$	= sum of the coupling forces in the radial direction
G_{zx}	= shear modulus of the truss
h	= height of the rhombic pyramid
l	= length of the rod
m	= mass of the lattice structure
r_0	= inner radius of the rod
r_1	= outer radius of the rod
r_2	= outer radius of the coupling flange
s	= semiperimeter of the shaded triangle
V	= volume of the rhombic pyramid
V_{cell}	= volume of the unit cell
V_{link}	= volume of the link
V_{node}	= volume of the node
V_{rod}	= volume of the rod
V_{strut}	= sum of the volumes of the struts contained within a unit cell
α	= opening angle at the base of the rhombic pyramid
β	= opening angle at the base of the rhombic pyramid
ε	= elastic strain
$\bar{\rho}$	= relative density of the octet-truss
σ	= stress

References

- [1] Neubert, J., Rost, A., and Lipson, H., 2014, “Self-Soldering Connectors for Modular Robots,” *IEEE Trans. Rob.*, **30**(6), pp. 1344–1357.
- [2] Rubenstein, M., Cornejo, A., and Nagpal, R., 2014, “Programmable Self-Assembly in a Thousand-Robot Swarm,” *Science*, **345**(6198), pp. 795–799.
- [3] Becker, A., Habibi, G., Werfel, J., Rubenstein, M., and McLurkin, J., 2013, “Massive Uniform Manipulation: Controlling Large Populations of Simple Robots With a Common Input Signal,” *IEEE/RSS International Conference on Intelligent Robots and Systems (IROS)*, Tokyo, Nov. 3–8, Tokyo, pp. 520–527.
- [4] Balkcom, D. J., and Mason, M. T., 2008, “Robotic Origami Folding,” *Int. J. Rob. Res.*, **27**(5), pp. 613–627.
- [5] Schenk, M., and Guest, S. D., 2011, “Origami Folding: A Structural Engineering Approach,” *Fifth International Meeting of Origami Science, Mathematics, and Education (Origami 5)*, Singapore, July 14–15, pp. 293–305.
- [6] Mueller, S., Im, S., Gurevich, S., Teibrich, A., Pfisterer, L., Guimbretière, F., and Baudisch, P., 2014, “WirePrint: 3D Printed Previews for Fast Prototyping,” *27th Annual ACM Symposium on User Interface Software and Technology (UIST)*, Honolulu, HI, Oct. 5–8.
- [7] Goldstein, S. C., Campbell, J. D., and Mowry, T. C., 2005, “Invisible Computing: Programmable Matter,” *Computer*, **38**(6), pp. 99–101.
- [8] Kodama, S., 2008, “Dynamic Ferrofluid Sculpture: Organic Shape-Changing Art Forms,” *Commun. ACM*, **51**(6), pp. 79–81.
- [9] Wakita, A., Nakano, A., and Kobayashi, N., 2011, “Programmable Blobs: A Rheologic Interface for Organic Shape Design,” *Fifth International Conference on Tangible, Embedded, and Embodied Interaction (TEI)*, Funchal, Portugal, Jan. 22–26, pp. 273–276.
- [10] Cheung, K. C., and Gershenfeld, N., 2013, “Reversibly Assembled Cellular Composite Materials,” *Science*, **341**(6151), pp. 1219–1221.
- [11] Groß, R., and Dorigo, M., 2008, “Self-Assembly at the Macroscopic Scale,” *Proc. IEEE*, **96**(9), pp. 1490–1508.
- [12] Fuller, R. B., 1961, “Octet Truss,” U.S. Patent No. 2,986,241.
- [13] Conway, J. H., Jiao, Y., and Torquato, S., 2011, “New Family of Tilings of Three-Dimensional Euclidean Space by Tetrahedra and Octahedra,” *Proc. Natl. Acad. Sci.*, **108**(27), pp. 11009–11012.
- [14] Li, Z., Balkcom, D. J., and Dollar, A. M., 2013, “Rigid 2D Space-Filling Folds of Unbroken Linear Chains,” *IEEE International Conference on Robotics and Automation (ICRA)*, Karlsruhe, Germany, May 6–10, pp. 551–557.
- [15] Deshpande, V. S., Ashby, M. F., and Fleck, N. A., 2001, “Foam Topology: Bending Versus Stretching Dominated Architectures,” *Acta Mater.*, **49**(6), pp. 1035–1040.
- [16] Griffith, S. T., 2004, “Growing Machines,” *Ph.D. dissertation*, Massachusetts Institute of Technology, Cambridge, MA.
- [17] Pevzner, P. A., Tang, H., and Waterman, M. S., 2001, “An Eulerian Path Approach to DNA Fragment Assembly,” *Proc. Natl. Acad. Sci. U.S.A.*, **98**(17), pp. 9748–9753.
- [18] Hawkes, E., An, B., Benbernou, N. M., Tanaka, H., Kim, S., Demaine, E. D., Rus, D., and Wood, R. J., 2010, “Programmable Matter by Folding,” *Proc. Natl. Acad. Sci.*, **107**(28), pp. 12441–12445.
- [19] Overvelde, J. T. B., de Jong, T. A., Shevchenko, Y., Becerra, S. A., Whitesides, G. M., Weaver, J. C., Hoberman, C., and Bertoldi, K., 2016, “A Three-Dimensional Actuated Origami-Inspired Transformable Metamaterial With Multiple Degrees of Freedom,” *Nat. Commun.*, **7**.
- [20] Nigl, F., Li, S., Blum, J. E., and Lipson, H., 2013, “Structure-Reconfiguring Robots: Autonomous Truss Reconfiguration and Manipulation,” *IEEE Rob. Autom. Mag.*, **20**(3), pp. 60–71.
- [21] Gershenfeld, N., Carney, M., Jenett, B., Calisch, S., and Wilson, S., 2015, “Macrofabrication With Digital Materials: Robotic Assembly,” *Archit. Des.*, **85**(5), pp. 122–127.
- [22] Cheung, K. C., Demaine, E. D., Bachrach, J. R., and Griffith, S., 2011, “Programmable Assembly With Universally Foldable Strings (Moteins),” *IEEE Trans. Rob.*, **27**(4), pp. 718–729.
- [23] Sproewitz, A., Asadpour, M., Bourquin, Y., and Ijspeert, A. J., 2008, “An Active Connection Mechanism for Modular Self-Reconfigurable Robotic Systems Based on Physical Latching,” *IEEE International Conference on Robotics and Automation (ICRA)*, Pasadena, CA, May 19–23, pp. 3508–3513.
- [24] Eckenstein, N., and Yim, M., 2014, “Design, Principles, and Testing of a Latching Modular Robot Connector,” *IEEE International Conference on Intelligent Robots and Systems (IROS)*, Chicago, IL, Sept 14–18, pp. 2846–2851.
- [25] Swensen, J. P., Nawroj, A. I., Pounds, P. E. I., and Dollar, A. M., 2014, “Simple, Scalable Active Cells for Articulated Robot Structures,” *IEEE International Conference on Robotics and Automation (ICRA)*, Hong Kong, China, May 31–June 7, pp. 1241–1246.
- [26] Deshpande, V. S., Fleck, N. A., and Ashby, M. F., 2001, “Effective Properties of the Octet-Truss Lattice Material,” *J. Mech. Phys. Solids*, **49**(8), pp. 1747–1769.
- [27] Dong, L., Deshpande, V., and Wadley, H., 2015, “Mechanical Response of Ti-6Al-4V Octet-Truss Lattice Structures,” *Int. J. Solids Struct.*, **60**, pp. 107–124.